UCLA
UCLA Previously Published Works

Title
Factors Influencing Central Lamina Cribrosa Depth: A Multicenter Study

Permalink
https://escholarship.org/uc/item/68n9z904

Journal
Investigative Ophthalmology & Visual Science, 59(6)

ISSN
0146-0404

Authors
Luo, Haomin
Yang, Hongli
Gardiner, Stuart K
et al.

Publication Date
2018-05-07

DOI
10.1167/iovs.17-23456

Peer reviewed

Factors Influencing Central Lamina Cribrosa Depth: A Multicenter Study

Haomin Luo,[1,2] Hongli Yang,[2] Stuart K. Gardiner,[3] Christy Hardin,[2] Glen P. Sharpe,[4] Joseph Caprioli,[5] Shaban Demirel,[3] Christopher A. Girkin,[6] Jeffrey M. Liebmann,[7] Christian Y. Mardin,[8] Harry A. Quigley,[9] Alexander F. Scheuerle,[10] Brad Fortune,[3] Balwantray C. Chauhan,[4] and Claude F. Burgoyne[2]

[1]Department of Ophthalmology, Second Xiangya Hospital, Central South University, Changsha, Hunan Province, P.R. China
[2]Devers Eye Institute, Optic Nerve Head Research Laboratory, Legacy Research Institute, Portland, Oregon, United States
[3]Devers Eye Institute, Discoveries in Sight Research Laboratories, Legacy Research Institute, Portland, Oregon, United States
[4]Ophthalmology and Visual Sciences, Dalhousie University, Halifax, Nova Scotia, Canada
[5]Jules Stein Eye Institute, David Geffen School of Medicine at University of California-Los Angeles, Los Angeles, California, United States
[6]Department of Ophthalmology, School of Medicine, University of Alabama at Birmingham, Birmingham, Alabama, United States
[7]Einhorn Clinical Research Center, Moise and Chella Safra Advanced Ocular Imaging Laboratory, New York Eye and Ear Infirmary of Mount Sinai Health System, New York, New York, United States
[8]Department of Ophthalmology, University of Erlangen, Erlangen, Germany
[9]Wilmer Eye Institute, Johns Hopkins University, Baltimore, Maryland, United States
[10]Department of Ophthalmology, University of Heidelberg, Heidelberg, Germany

PURPOSE. To quantify the influence of ocular and demographic factors on central laminar depth (LD) in healthy participants.

METHODS. A total of 362 normal subjects underwent optical coherence tomography (OCT) enhanced depth imaging of the optic nerve head (ONH) with a 24 radial B-scan pattern aligned to the fovea–to–Bruch's membrane opening (BMO) axis. BMO, anterior lamina, anterior scleral canal opening (ASCO), Bruch's membrane (BM), and the peripapillary scleral surface were manually segmented. The extent of laminar segmentation was quantified within 72 ASCO subsectors. Central LD was quantified relative to four reference planes: BMO, ASCO, BM, and scleral. The effects of age, sex, ethnicity, IOP, BMO area, ASCO area, and axial length on LD were assessed.

RESULTS. Laminar visibility was most consistent within the central ASCO (median 89%, range, 69%–95%). LD_{BMO} and LD_{BM} were significantly shallower in eyes with greater age, BMO area, and axial length and in females. LD_{ASCO} was shallower in eyes with greater ASCO area and axial length and in European and Hispanic descent compared to African descent eyes. LD_{Sclera} behaved similarly, but was not associated with axial length. BMO and ASCO area were not different between African descent and European descent eyes.

CONCLUSIONS. Central LD was deeper in African descent eyes and influenced least by age, axial length, and sex, but more by ASCO area, when measured relative to the ASCO and sclera. However, the magnitude of these effects for all four reference planes was small, and their clinical importance in the detection of glaucoma and its progression remains to be determined.

Keywords: Bruch's membrane, optic nerve head, optical coherence tomography, glaucoma, laminar depth

Vision loss in glaucoma involves retinal ganglion cell (RGC) axon injury within the optic nerve head (ONH) tissues followed by RGC death. However, the optic neuropathy of glaucoma also involves deformation and remodeling of the connective tissues of the lamina cribrosa, scleral canal wall, and peripapillary sclera[1] in a process that is clinically known as "glaucomatous cupping."[2,3] As clinical ONH imaging has penetrated the ONH surface, ONH phenotyping in glaucoma has evolved from clinical estimates of cup–disc ratio[4] to optical coherence tomography (OCT) measurements of rim width[5–9]

and laminar depth (LD) relative to both Bruch's membrane opening (BMO) and the peripapillary sclera.[10–19]

Posterior (outward) laminar deformation can be detected by OCT prior to retinal nerve fiber layer (RNFL) thinning in monkey experimental glaucoma,[20] but has not been shown to occur in any other monkey optic neuropathy model.[21–23] Glaucoma patients demonstrate deeper laminas[2,12–16,24,25] and larger laminar curvature[11,24,26] compared to healthy subjects. The depth of the lamina in glaucoma patients relative to BMO, peripapillary Bruch's membrane (BM), and peripapillary scleral
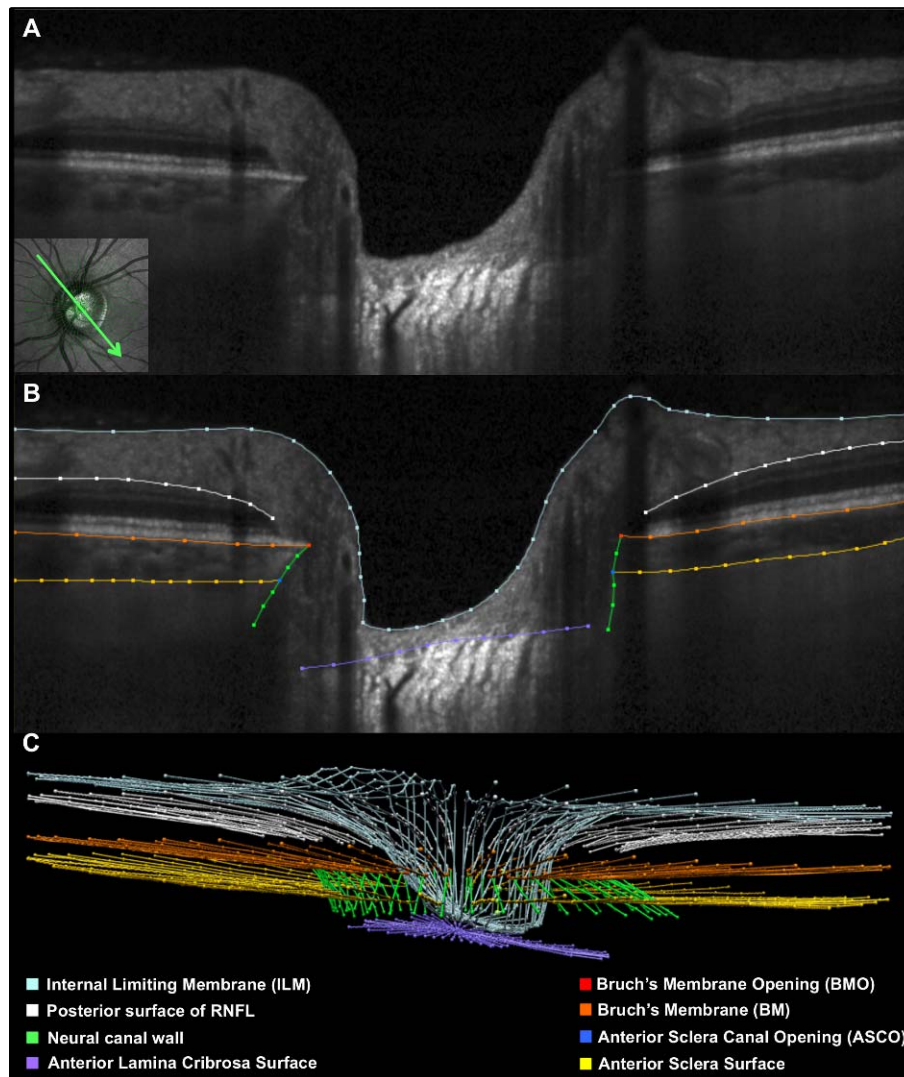
FIGURE 1. Manual segmentation of each radial B-scan. (**A**) A representative 15° radial B-scan is shown, with its location depicted in the inlayed infrared image (*bottom left*). (**B**) Manually segmented B-scan shown in (**A**). *Light blue lines/points* indicate the ILM, *white lines/points* the posterior surface of the RNFL, *orange lines/points* are the posterior surface of the BM/RPE complex (BM), *gold lines/points* are anterior surface of sclera. *Green lines/points* are neural canal wall, *purple lines/points* are anterior lamina cribrosa surface. *Red points* are the BMO, and *blue points* are the ASCO. (**C**) Point cloud of segmented points from the complete set of 24 radial B-scans obtained for this ONH.

reference planes has been shown to vary with age[13,14,27] and by glaucoma disease severity.[13,15,16,27] In a recent longitudinal study, glaucoma patients demonstrated serial changes in laminar depth as commonly as ONH rim and RNFL changes, but often these phenomena occurred in different eyes.[17] In a second longitudinal study,[19] both anterior and posterior laminar depth changes were linked to increased rates of visual field progression, with the direction of change determined by whether a BMO or a scleral reference plane was used to make the measurement.

A consistent strategy for characterizing central laminar depth is necessary to most robustly evaluate its contribution to the OCT detection of glaucoma. It is also essential to the task of incorporating the ONH connective tissues (rather than just the rim and/or RNFL) into ONH phenotyping for genetic studies and ONH glaucoma disease staging. To date, several studies have reported laminar depth in healthy human eyes, using BMO, peripapillary BM, and peripapillary scleral reference planes.[10–12,18,24] However, there has been no attempt to segment the anterior scleral canal opening (ASCO)[24,28] (Fig. 1)

so as to incorporate an ASCO-based definition of the central lamina (Fig. 2) and an ASCO reference plane (Fig. 3) into the OCT characterization of laminar depth.

The purpose of the present study was to measure the parameter central laminar depth in a large group of healthy eyes relative to four separate reference planes, BMO (LD_{BMO}), ASCO (LD_{ASCO}), peripapillary BM (LD_{BM}), and peripapillary sclera (LD_{Sclera}) (Fig. 3), and to quantify and compare the influence of age, axial length, ethnicity, sex, IOP, BMO area, and ASCO area on each version of the parameter.

METHODS

Conventions

The parameter LD is positive when the lamina is posterior (external) to its reference plane, increases (or is deeper), the farther it is from the reference plane, and decreases (or is shallower), the closer it is located to its reference plane. Factors that have "positive" and "negative" effects on LD
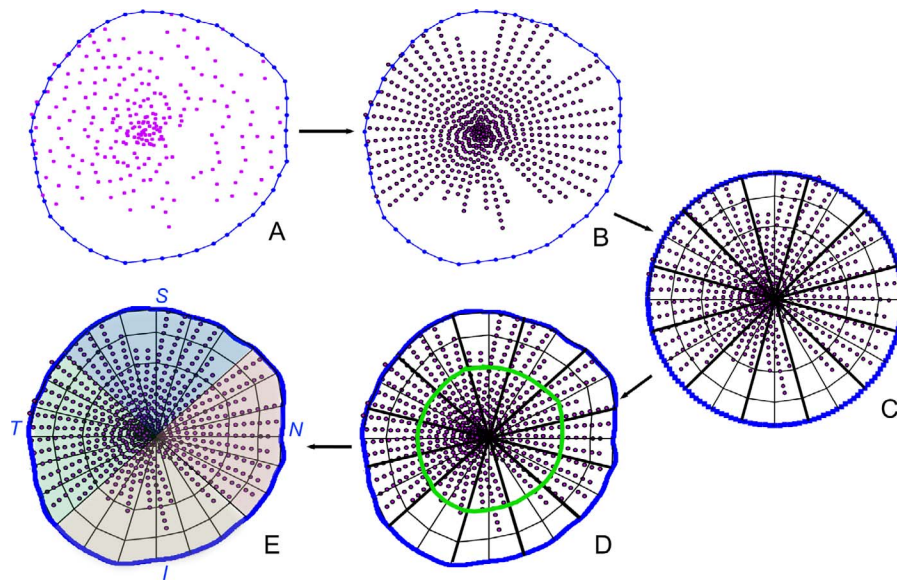
FIGURE 2. The extent of laminar segmentation and the central region of the lamina are both defined relative to the anterior sclera canal opening (ASCO). (**A**) Segmented anterior laminar surface points (*purple*) are projected onto an ASCO reference plane that is based upon a continuous B-spline (*blue line*) fit to the segmented ASCO points (*blue*). (**B**) Segmented points are resampled (now in *purple with black border*) to be equidistant along the segmented portion of the anterior lamina within each B-scan. (**C**) The ASCO B-spline is scaled into a unit circle and divided into twelve 30° sectors and 72 subsectors of equal area, which are positioned relative to the fovea-to-BMO axis (not shown). Each segmented point is scaled into the same unit circle. Subsectors containing ≥1 segmented point are defined as "visible." (**D**) The unit circle and contained segmented points are transformed back into the original ASCO space. The parameter central laminar depth consistently samples the central 24 ASCO subsectors (*green outline* in **D**) regardless of the reference plane used for the depth measurement (see Fig. 3). (**E**) Laminar visibility was quantified by summing the number of visible subsectors within the central 24 subsectors (*green outline* in **D**) and within superior (S, *blue shade*), inferior (I, *orange shade*), nasal (N, *pink shade*), and temporal (T, *green shade*) quadrants.

therefore correlate to "deeper" and "shallower" laminas, respectively.

Participants

A total of 362 healthy individuals participated in this study. Two hundred forty-six self-identified European descent participants were recruited in five centers (one center in Canada [Halifax, NS], two in the United States [Portland, OR, and Birmingham, AL], and two in Germany (Erlangen and Heidelberg) as reported previously.[9] A total of 116 additional Hispanic descent, African descent, Asian descent, and Native American descent participants were recruited separately in three centers in the United States (Baltimore, MD; New York, NY; Los Angeles, CA). The number of participants recruited for each ethnicity was designed to achieve a normative database that is representative of the ethnic composition of the US population[29] as mandated by the U.S. Food and Drug Administration (FDA). Consent documents preapproved by the institutional review board of each participating institution were signed and dated by the participants as the first step of their enrollment into the study. The study followed the tenets of the Declaration of Helsinki for research involving human participants.

At the first visit, a medical and ophthalmic history was obtained, followed by anterior segment examination, external examination, Van Herrick angle assessment, and crystalline lens evaluation with a slit lamp; visual acuity measurement with a standard Snellen or Early Treatment Diabetic Retinopathy Study (ETDRS) chart; refraction; central keratometry with an autokeratometer, a corneal topographer, or a manually operated keratometer; and axial length with ultrasound biometry measurement. Visual field examination was then conducted with standard automated perimetry (Humphrey Field Analyzer [Carl Zeiss Meditec, Dublin, CA, USA], with the 24–2 Swedish Interactive Thresholding Algorithm), repeated

once if deemed unreliable or outside normal limits (see below). OCT examination (see below), ophthalmoscopic examination of the posterior pole, and ONH stereophotography were also performed. Following the OCT examination, Goldmann tonometry and pachymetry were performed.

Inclusion criteria included (1) age between 18 and 90 years old; (2) negative history of glaucoma and intraocular pressure ≤ 21 mm Hg; (3) best-corrected visual acuity ≥ 20/40, spectacle refraction less than ±6.00-diopter (D) sphere and ±2.00-D cylinder; (4) visual field Glaucoma Hemifield Test and mean deviation within normal limits. Exclusion criteria included (1) unusable disc stereo photos or insufficient OCT image quality (quality score < 20); (2) clinically abnormal appearance of the optic disc; (3) any intraocular surgery (except uncomplicated cataract surgery) or vitreous, retinal, choroidal, or neuroophthalmologic disease; (4) self-identified ethnic group other than European descent, Hispanic descent, African descent, Asian descent, or Native American descent. While all test procedures were performed on both eyes of each participant, only one eye was randomized (if both eyes were available for randomization) for manual delineation, data generation, and analysis. In those participants in whom one eye was excluded from the study, the other eye was included.

OCT Image Acquisition and Segmentation

The ONH, peripapillary RNFL, and macula were imaged with spectral-domain OCT (Spectralis; Heidelberg Engineering GmbH, Heidelberg, Germany, software version Heyex 1.9.10.0). The participant was positioned comfortably, and the refractive correction and keratometry values were entered into the instrument database to ensure accurate transverse scaling of all measurements.

Prior to image acquisition, the operator first manually defined the location of the fovea using a live B-scan, whose
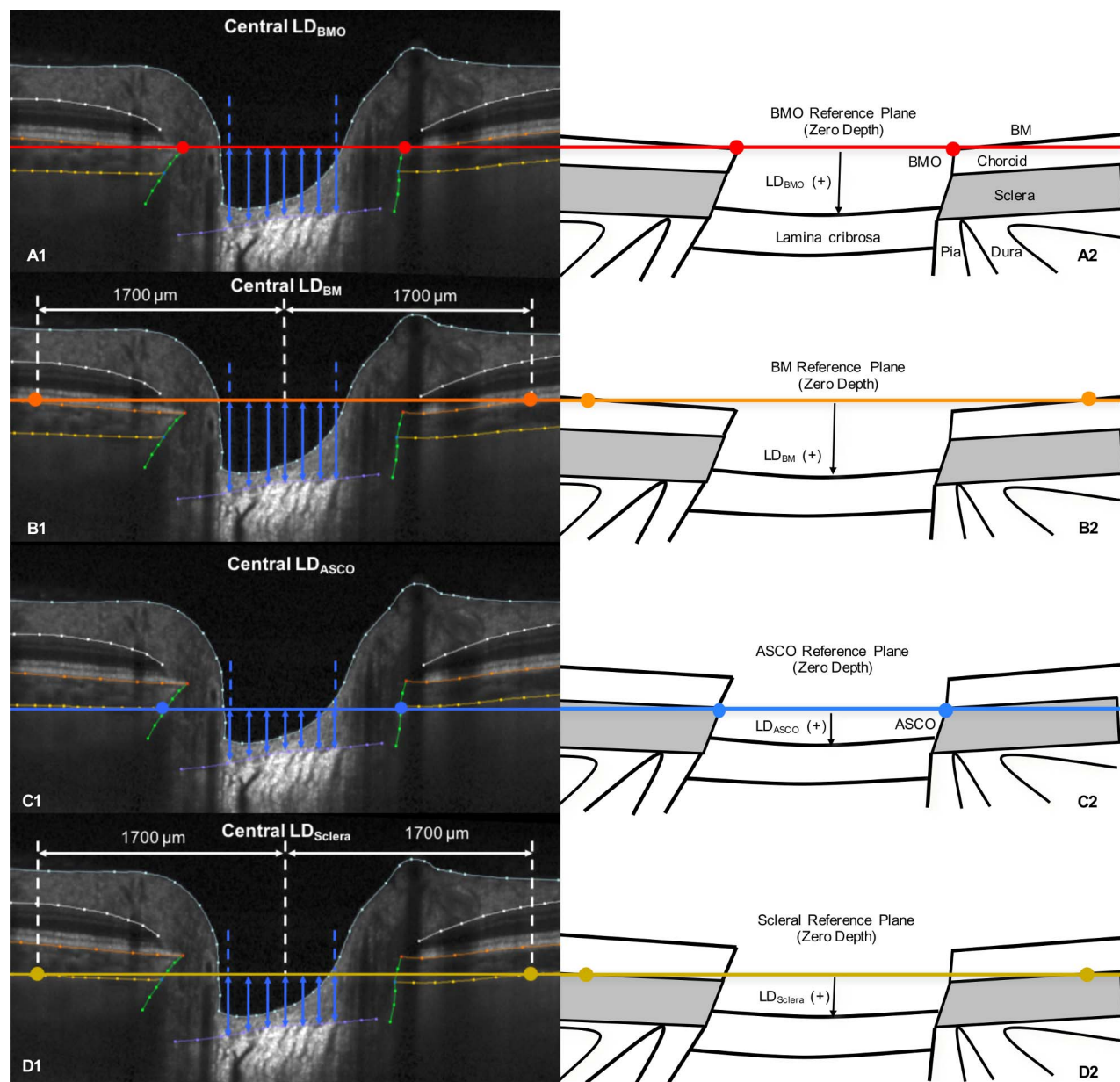
FIGURE 3. The parameter central laminar depth (LD) measures laminar depth within the central anterior scleral canal opening (ASCO) relative to four reference planes (*left*) and is schematically depicted on the *right*. (**A1**, **A2**) Central LD_{BMO} is the mean depth of the segmented anterior surface points within the central 24 ASCO subsectors, measured relative to the BMO (*two red points*) reference plane, which is shown in cross section as a *red line*. (**B1**, **B2**) Central LD_{BM} is the mean depth of the same central ASCO segmented points measured relative to a BM reference plane, defined by the segmented BM points (*orange dots*) located 1700 μm away from the BMO centroid and seen in cross section as an *orange line*. (**C1**, **C2**) Central LD_{ASCO} is the mean depth of the same central ASCO segmented points (*blue dots*) measured relative to an ASCO reference plane seen in cross section as a *blue line*. (**D1**, **D2**) Central LD_{Sclera} is the mean depth of the same central ASCO segmented points measured relative to a scleral reference plane, defined by the segmented anterior scleral points (*gold dots*) located 1700 μm away from the ASCO centroid and seen in cross section as a *gold line*.

position was moved accordingly. Then the operator centered the imaging field on the ONH, where the two BMO points in each of two perpendicular ONH radial B-scans were identified. These points were used to derive the eye-specific, fovea-to-BMO (FoBMO) axis for acquisition of all subsequent scans. The complete ONH imaging pattern consisted of 24 radially equidistant, 15° B-scans (768 A-lines each) centered on BMO and acquired in enhanced depth imaging (EDI)[30] mode, with an average of 25 repetitions each. The quality score was at least 20 for all ONH scans included in this study.

Our strategy for OCT ONH image manual segmentation has been described previously.[20,31,32] The segmented surfaces and landmarks were based on previous direct comparisons between SD-OCT B-scans and matched histologic sections,[32] recent comparisons to three-dimensional (3D) histomorphometric reconstructions (Zangalli C, et al. *IOVS* 2014;55:ARVO E-Abstract 4747), and our previous publications on SD-OCT laminar visualization[33] and longitudinal change detection.[20,34] Raw OCT volumes along with automatic segmented BMO points and internal limiting membrane (ILM) lines were

exported from the device software and imported into our custom 3D visualization and segmentation software (ATL 3D Suite).[35] ONH and peripapillary landmarks were manually segmented in every radial B-scan (24 total) of each OCT volume (Fig. 1). Segmented landmarks (Fig. 1) included the ILM; posterior surface of the RNFL; posterior surface of the Bruch's membrane/retinal pigment epithelium (BM/RPE) complex; Bruch's membrane opening, defined as the innermost termination of the OCT-detected BM/RPE complex on either side of neural canal; neural canal wall (defined as the inner boundary of the connective tissues separating the RGC axon bundles from the choroid and sclera, extending from BMO to the pial sheath); anterior lamina cribrosa surface; anterior scleral surface; and the ASCO. The ASCO was segmented on each side of the canal by visually projecting the plane of the immediate peripapillary anterior scleral surface through the neural canal wall and marking their intersection. Manual correction of the automatically segmented BMO and ILM points was necessary only in less than 5% of all B-scans. All manual segmentations and corrections used in this study were done within the Devers Eye Institute, Optic Nerve Head Research Laboratory.

Extent of Anterior Laminar Surface Segmentation Relative to the ASCO

To most fairly assess how much of the lamina in a given eye was visualized well enough to have its anterior surface manually segmented in a manner that could be consistently applied to each eye, we quantified the extent of laminar segmentation within 72 ASCO subsectors (5° sampling interval) as well as central, midperipheral, and peripheral ASCO regions as described in Figure 2 (Matlab version 7.3.0.267; The MathWorks, Natick, MA, USA). For each OCT data set, a plane was fit to the 48 segmented ASCO points (the ASCO reference plane) utilizing a least mean square error restraint.[27,28,32] To compensate for interobserver variability in the density of the anterior laminar segmentation points, for each OCT data set, the anterior laminar surface points within each radial B-scan were resampled to be equidistant (50 μm apart) along the segmented portion of the anterior lamina, and projected to the ASCO reference plane. To make the process identical for all eyes regardless of eye-specific ASCO anatomy, the projected ASCO points were transformed into a unit circle within the ASCO reference plane and divided into twelve 30° (clock-hour) sectors and 72 subsectors of equal area, which were positioned relative to the FoBMO axis. Each resampled anterior lamina cribrosa point was then scaled to the same unit circle. Subsectors containing ≥1 segmented point were defined as "visible." Laminar visibility was reported for the whole ASCO, the central, midperipheral, and peripheral ASCO, and the superior, inferior, temporal, and nasal ASCO quadrants by totaling the number of visible subsectors in each (Fig. 2).

Central Laminar Depth

Because the central lamina was most consistently visualized (see Results), our analyses focused on the parameter central LD, which was defined to be the mean depth of the segmented points within the central 24 ASCO subsectors (green outline in Fig. 2D) regardless of the reference plane used for the depth measurement (Fig. 3). Quantification of all parameters derived from the manually segmented points was performed within custom software (Matlab version 7.3.0.267). All left eye data were converted to right eye configuration for analysis and presentation.[36]

BMO, ASCO, Peripapillary BM, and Peripapillary Scleral Reference Planes

A BMO reference plane was determined based on the 48 BMO points (2 points in each of 24 radial B-scans) as described in Figure 2 for the ASCO reference plane. Peripapillary BM and peripapillary scleral reference planes were separately defined by fitting a plane to 48 points 1700 μm distal to the BMO centroid (for the BM points) and ASCO centroid (for the scleral points) (Fig. 3). Reference plane nonplanarity (a measure of the "flatness" of its constituent points) was defined to be the mean of the absolute distance of all segmented points from the fitted reference plane.

Quantification of BMO and ASCO Area

BMO and ASCO area were calculated as the area encompassed by the projection of the BMO and ASCO points to their respective reference planes.

Interobserver Reproducibility

Interobserver segmentation reproducibility was assessed for each parameter by having four manual segmentation technicians (now referred to as "observers") each segment the same eight OCT data sets. The eight OCT data sets came from one eye of eight participants randomly selected from three centers (two European descent subjects from Halifax; three European descent subjects from Heidelberg; one Asian descent, one African descent, and one Hispanic descent subject from Baltimore). For each OCT data set, global values for the four LD parameters, BMO area, ASCO area, and reference plane nonplanarity were generated for each observer. All OCT segmentations were performed by experienced observers within the Devers Eye Institute, Optic Nerve Head Research Laboratory in Portland, Oregon, which is separate from the Devers Eye Institute Clinical Study, image acquisition site.

Statistical Analysis

All statistical analyses were performed in R version 3.1.3 (The R Foundation for Statistical Computing, Vienna, Austria). Intraclass correlation coefficients (ICC) between observers for each global parameter (i.e., one value per subject per observer) were calculated using a 2-way analysis of variance (ANOVA).[37,38] A Poisson regression model was used to relate laminar visibility with age adjusting for ASCO area, axial length, sex, and ethnicity using a χ^2 test. Univariate regression models were formed to relate central LD with age, BMO area (for LD_{BMO} and LD_{BM}), ASCO area (for LD_{ASCO} and LD_{Sclera}), axial length, imaging day IOP, sex, and ethnicity. The significance and magnitude of the effects of age, BMO area, ASCO area, axial length, IOP, sex, and ethnicity on each laminar depth parameter were assessed by calculating the proportion of the total variance (R^2) explained by the independent variables in an ANOVA with a linear regression model. Coefficients of the effects were assessed by a multivariable linear regression model. The raw and adjusted rate of change of laminar depth versus age, BMO area, ASCO area, axial length, and IOP were calculated for each laminar depth parameter. Statistical significance was assumed when $P \leq 0.05$.

RESULTS

Demographic and clinical characteristics for all 362 participants are summarized in Table 1. This cohort included 246 (68.0%) European descent, 47 (13.0%) Hispanic descent, 47 (13.0%) African descent, 19 (5.2%) Asian descent, and 3 (0.8%)

TABLE 1. Demographic and Ocular Characteristics of the Study Participants

Characteristics	All Subjects, $n = 362$	Subjects With Visible Sclera,* $n = 357$	Subjects With Visible Lamina, $n = 344$	Subjects With Visible Sclera and Lamina, $n = 339$
Sex, female, n (%)	202 (55.8)	201 (56.3)	197 (57.3)	196 (57.8)
Ethnicity				
European descent, n (%)	246 (68.0)	244 (68.3)	234 (68.0)	232 (68.4)
Hispanic descent, n (%)	47 (13.0)	46 (12.9)	44 (12.8)	43 (12.7)
African descent, n (%)	47 (13.0)	45 (12.6)	45 (13.1)	43 (12.7)
Asian, Native American, n (%)	22 (6.0)†	22 (6.2)	21 (6.1)	21 (6.2)
Left eye, n (%)	181 (50.0)	180 (50.4)	169 (49.1)	168 (49.6)
Age, y (SD)	50.6 (17.5)	50.6 (17.6)	50.5 (17.6)	50.5 (17.6)
Axial length, mm (SD)	23.7 (0.96)	23.7 (0.96)	23.7 (0.95)	23.7 (0.95)
IOP, mm Hg (SD)	15 (2.70)	14.5 (2.72)	14.5 (2.69)	14.5 (2.71)
CCT, μm (SD)	555 (32.6)	556 (32.8)	554 (32.9)	555 (33.0)
Refraction, D (SD)	−0.38 (1.90)	−0.39 (1.90)	−0.38 (1.88)	−0.39 (1.90)
Cylinder, D (SD)	−0.18 (0.67)	−0.18 (0.68)	−0.16 (0.66)	−0.16 (0.66)
Corneal curvature, mm (SD)	7.74 (0.27)	7.74 (0.27)	7.74 (0.27)	7.74 (0.27)

IOP, intraocular pressure; CCT, central corneal thickness; D, degree; SD, standard deviation.
* See Methods for description.
† 19 (5.2%) Asian and 3 (0.8%) Native American.

Native American descent participants. There were 202 (55.8%) female participants and 181 (50%) left eyes. Eighteen participants were excluded from the analysis of LD_{BMO}, LD_{BM}, and LD_{ASCO} and 23 participants were excluded from the analysis of LD_{Sclera} because of poor laminar (18 participants) and scleral (5 participants) visualization by OCT. The mean age (standard deviation and range) of all 362 participants was 50.6

FIGURE 4. Frequency of anterior lamina cribrosa surface delineation by anterior scleral canal opening (ASCO) subsector in 362 healthy eyes. *Yellow lines* demarcate 30°, fovea-to-BMO ASCO sectors[8] that are subdivided into 72 ASCO subsectors of equal area. Data are plotted in right eye orientation relative to a unit circle representation of the ASCO of each study eye (*blue outline*) (see Fig. 2). For a given eye, at least one segmented point per subsector was required for that subsector to achieve "visualization." Frequency data (*gray scale*) represent the percent of 362 eyes in which an individual subsection was visualized. The anterior laminar surface was most frequently segmented within the central (*green circle*) and temporal subsectors of the ASCO.

(17.5 and 20-90) years. There were an approximately equal number of participants within each decade group except those aged ≥ 70 years (decade 21-30 years: 58 participants; decade 31-40 years: 57 participants; decade 41-50 years: 64 participants; decade 51-60 years: 66 participants; decade 61-70 years: 58 participants; decade 71-80 years: 42 participants; and decade 81-90 years: 17 participants).
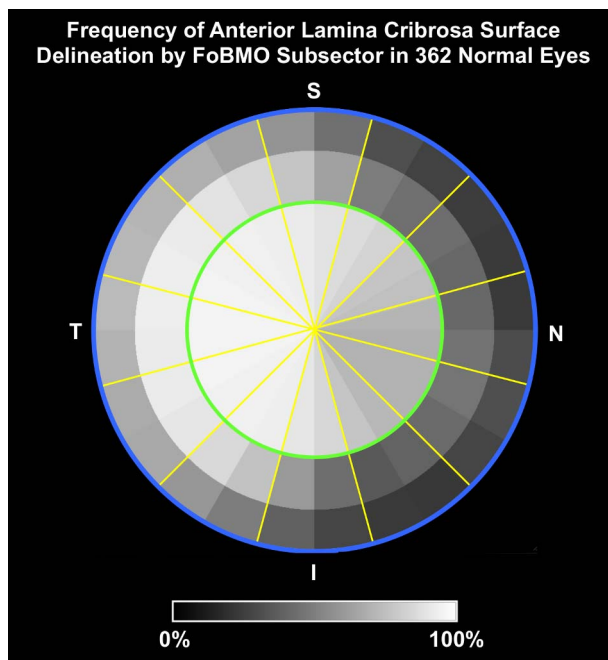
Laminar Visibility

The percentage of study eyes in which the anterior laminar surface was visible by ASCO region and subsector is reported in Figure 4. The median number of subsectors in which the lamina could be segmented was 89% (range, 69%-95%) for the central subsectors, 61% (range, 35%-93%) for the midperipheral subsectors, and 41% (range, 22%-73%) for the peripheral subsectors. In general, the lamina was most commonly visible within the central and temporal subsectors. Eye-specific laminar visibility ranged from 19% to 100% of the 72 ASCO subsectors (mean: 69%, median 68%) for the eyes included in the laminar depth analysis. Total laminar visibility (the number of visible subsectors among the 72 ASCO subsectors) significantly increased with age (0.3% per year, $P < 0.0001$). This increase was greatest within the nasal (0.56% increase per year, $P < 0.0001$) and inferior subsectors (0.53% increase per year, $P < 0.0001$), was less in the superior quadrant (0.2% increase per year, $P = 0.02$), and did not demonstrate significant associations with the temporal quadrant or central ASCO region.

Interobserver Reproducibility

No significant differences between observers were observed for any of the global parameters in this study. Reproducibility was high for most parameters (between observer ICC values greater than 0.89) except for the parameter scleral reference plane nonplanarity, for which it was only fair (ICC value 0.47).[37,38]

Laminar Depth, BMO Area, and ASCO Area

The population means for each parameter, as well as the values for their median, 95% confidence interval (CI), and range, are reported in Table 2. Scatter plots and univariate

TABLE 2. Population Means and Distribution by Parameter

Parameter	Mean	SD	Minimum	5% Percentile	Median	95% Percentile	Maximum
Central LD_{BMO}, μm	402	91	209	264	393	550	772
Central LD_{BM}, μm	498	123	213	312	495	703	977
Central LD_{ASCO}, μm	309	88	107	176	302	458	684
Central LD_{Sclera}, μm	332	96	103	193	328	502	665
Axial length, mm	23.74	0.95	21.41	22.32	23.68	25.47	26.44
BMO area, mm^2	1.832	0.384	1.047	1.239	1.808	2.529	3.46
ASCO area, mm^2	2.229	0.433	1.244	1.536	2.19	2.938	3.966
BMO nonplanarity,* μm	10	4	2	4	9	18	31
BM nonplanarity,* μm	8	4	2	4	8	15	25
ASCO nonplanarity,* μm	10	4	3	5	10	18	33
Scleral nonplanarity,* μm	16	5	5	9	15	26	41

* Nonplanarity of the reference plane based on this anatomic landmark.

linear regression analyses of each LD parameter with age, BMO or ASCO area, axial length, and imaging day IOP are reported in Figures 5, 6, 7, and 8, respectively. Multivariable regression coefficients for the effects of age, BMO area, ASCO area, sex, axial length, IOP, and ethnicity on each LD parameter are reported in Table 3. Multivariable regression coefficients for the effects of age, sex, axial length, and

ethnicity on BMO area and ASCO area are reported in Table 4.

Within univariate regression models (R^2 values for each model ranging from 0.01 to 0.04), all associations were weak even when they achieved significance. Increased age was significantly associated with shallowing of LD_{BMO} and LD_{BM} but not with LD_{ASCO} and LD_{Sclera} (Fig. 5), and increased BMO area
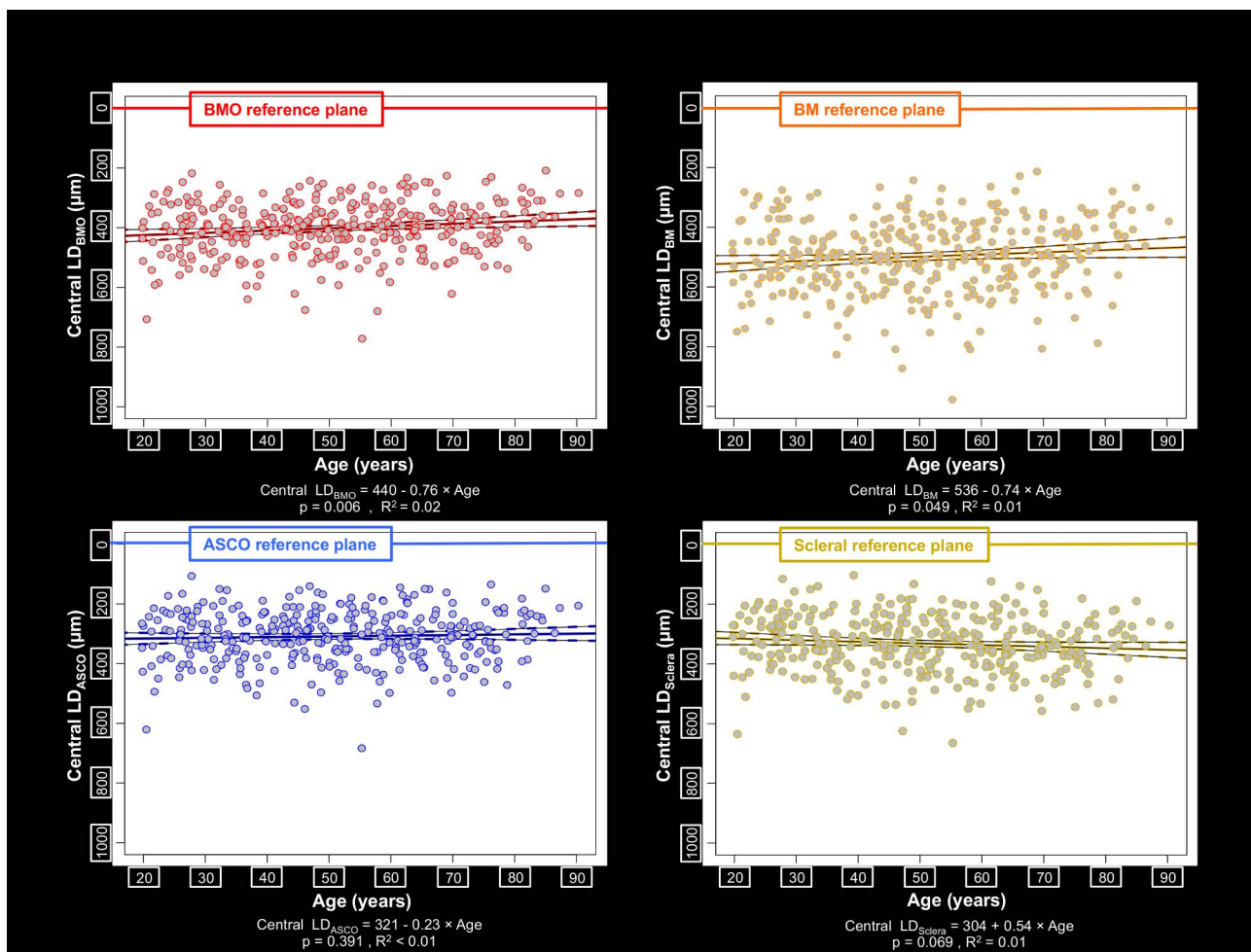

FIGURE 5. Scatter plot and univariate linear regression for central laminar depth and age. The relationship between central laminar depth and age is shown with points *shaded gray* and their circumference colored according to their reference plane. *Solid colored lines*: fitted linear regression lines; *dotted colored curves*: the 95% CI of the regression lines; *gray circles with colored border*: individual values. The slope of the regression line achieved significance ($P \leq 0.05$) for LD_{BMO} and LD_{BM}. The regression equations are $LD_{BMO} = 440 - 0.76 \times Age$ ($P = 0.006$; $R^2 = 0.02$) and $LD_{BM} = 536 - 0.74 \times Age$ ($P = 0.049$; $R^2 = 0.01$).
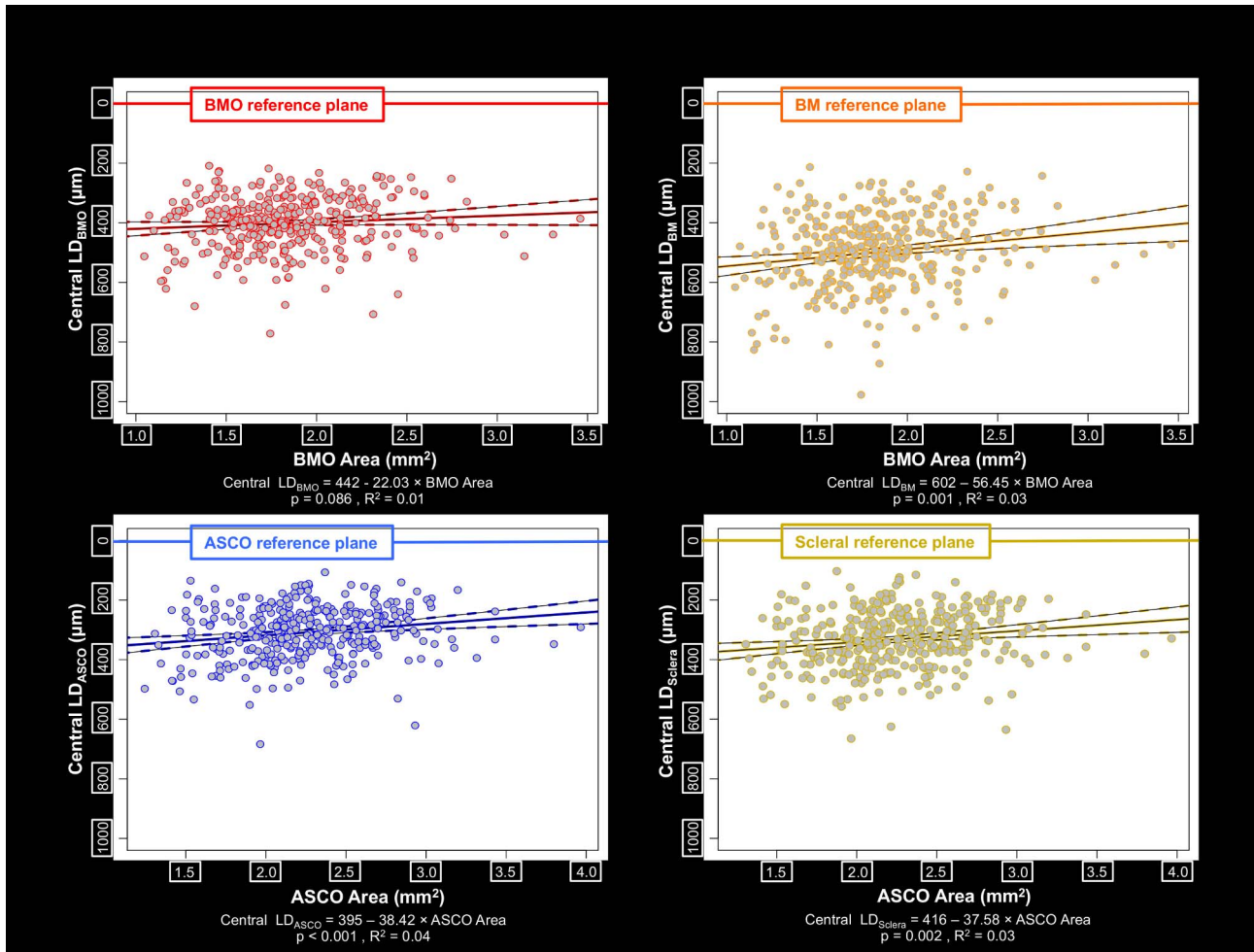
FIGURE 6. Scatter plot and univariate linear regression for central laminar depth and BMO or ASCO area. The relationship between laminar depth and BMO or ASCO area is shown with points *shaded gray* and their circumference colored according to their reference plane. *Solid colored lines*: fitted linear regression lines; *dotted colored curves*: the 95% CI of the regression lines; *gray circles with colored border*: individual values. The slope of the regression line achieved significance ($P \leq 0.05$) for LD_{BM}, LD_{ASCO}, and LD_{Sclera}. The regression equations are $LD_{BM} = 602 - 56.45 \times$ BMO Area ($P = 0.001$, $R^2 = 0.03$), $LD_{ASCO} = 395 - 38.42 \times$ ASCO Area ($P < 0.001$, $R^2 = 0.04$), and $LD_{Sclera} = 416 - 37.58 \times$ ASCO Area ($P = 0.002$, $R^2 = 0.03$).

TABLE 3. Multivariable Regression Coefficients by Effect and Central Laminar Depth (LD) Parameter

Parameter	Central LD_{BMO} Coefficient	SE	Central LD_{BM} Coefficient	SE	Central LD_{ASCO} Coefficient	SE	Central LD_{Sclera} Coefficient	SE
Intercept	**882.13**	130.11	**1371.28**	171.04	**705.27**	127.08	**593.75**	139.83
Age	**−0.94**	0.27	**−1.09**	0.36	−0.48	0.27	0.35	0.3
BMO area	**−25.86**	12.59	**−58.15**	16.55	NA	NA	NA	NA
ASCO area	NA	NA	NA	NA	**−39.48**	10.85	**−33.85**	12.05
Axial length	**−16.46**	5.13	**−29.39**	6.75	**−12.61**	5.02	−10.27	5.52
IOP	1.27	1.76	2.28	2.31	2.2	1.72	**4.09**	1.89
Sex,‡ male vs. female	**25.4**	9.72	**36.22**	12.77	17.58*	9.49	19.94†	10.48
Ethnicity§								
European and Hispanic descent vs. African descent	−26.84	14.13	**−70.27**	18.58	−26.99	13.8	**−31.15**	15.44
Asian and Native American descent vs. African descent	−33.58	23.36	**−83.53**	30.71	−28.42	22.67	−37.03	25.04

Bolded values indicate statistical significance, $P \leq 0.05$. SE, standard error.
* $P \leq 0.07$.
† $P \leq 0.06$.
‡ Parameter in male participants was compared to the same parameter in reference female participants.
§ Parameter in European and Hispanic descent and Asian and Native American descent participants was compared to the same parameter in reference African descent participants separately.
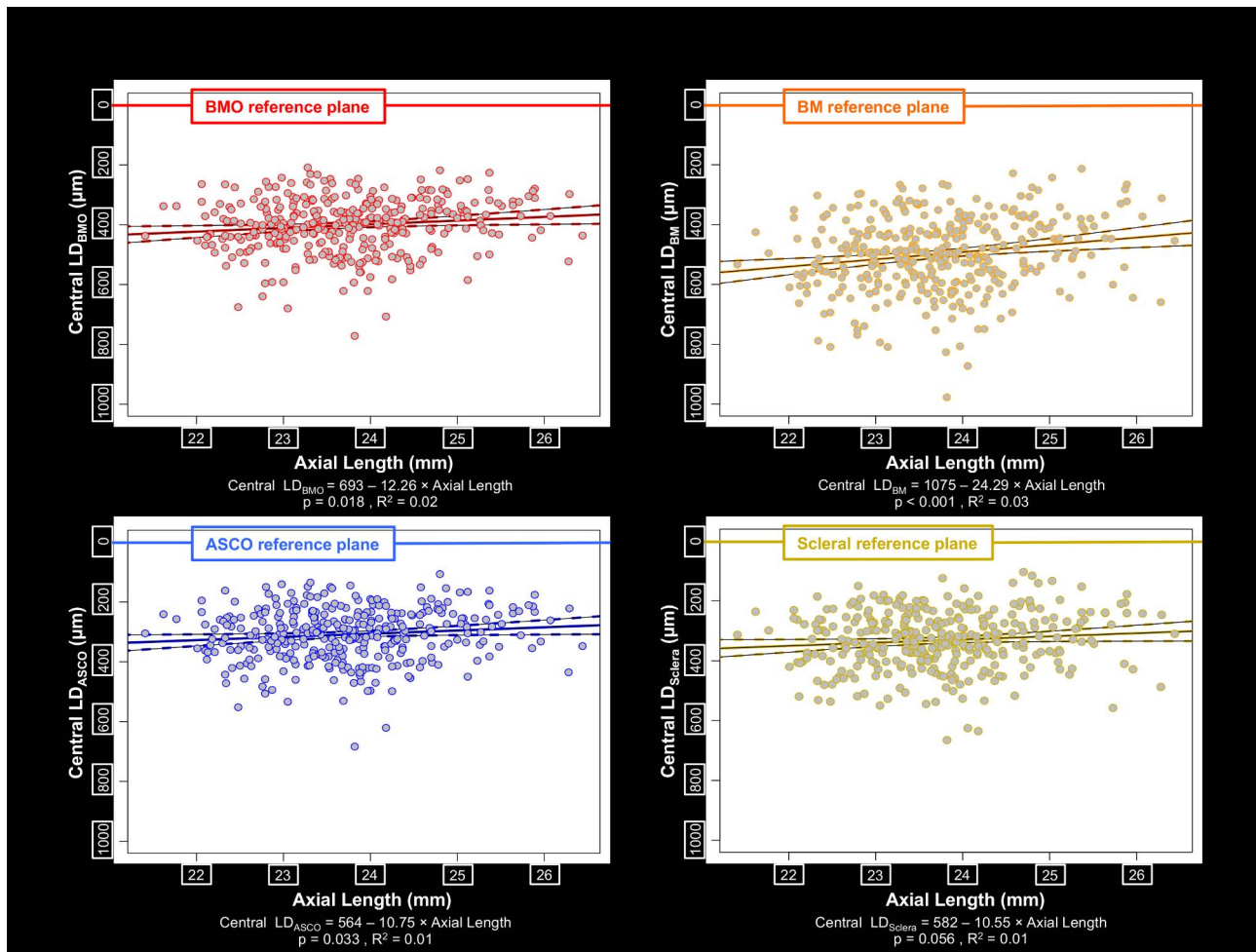
FIGURE 7. Scatter plot and univariate linear regression of central laminar depth with axial length. The relationship between central laminar depth and axial length is shown, with points *shaded gray* and their circumference colored according to their reference plane. *Solid colored lines*: fitted linear regression lines; *dotted colored curves*: the 95% CI of the regression lines; *gray circles with colored border*: individual values. The slope of the regression line achieved significance ($P \leq 0.05$) for LD_{BMO}, LD_{BM}, and LD_{ASCO}. The regression equations are $LD_{BMO} = 693 - 12.26 \times$ Axial Length ($P = 0.018$, $R^2 = 0.02$) and $LD_{BM} = 1075 - 24.29 \times$ Axial Length ($P < 0.001$, $R^2 = 0.03$), $LD_{ASCO} = 564 - 10.75 \times$ Axial Length ($P = 0.033$, $R^2 = 0.01$).

TABLE 4. Multivariable Regression Coefficients by Effect and by BMO Area and ASCO Area

Parameter	BMO Area		ASCO Area	
	Coefficient	SE	Coefficient	SE
Intercept	**1.695**	0.526	**2.018**	0.593
Age	**−0.002**	0.001	**−0.004**	0.001
Axial length	0.009	0.022	0.018	0.024
Sex,* male vs. female	0.027	0.041	−0.058	0.046
Ethnicity†				
European and Hispanic descent vs. African descent	0.023	0.06	0.025	0.067
Asian and Native American descent vs. African descent	**0.236**	0.098	0.079	0.111

Bolded values indicate statistical significance, $P \leq 0.05$. SE, standard error.

* Parameter in male participants was compared to the same parameter in reference female participants.

† Parameter in European and Hispanic descent, Asian and Native American descent participants was compared to the same parameter in reference African descent participants separately.

was associated with shallowing of LD_{BM} but not LD_{BMO}, and increased ASCO area was associated with shallowing of both LD_{ASCO} and LD_{Sclera} (Fig. 6). Increased axial length was significantly associated with shallowing of LD_{BMO}, LD_{BM}, and LD_{ASCO} (Fig. 7). Higher imaging day IOP was significantly associated with a deeper LD_{Sclera} (Fig. 8), but was not significantly associated with any other LD parameter.

Within a multivariable linear regression model (Table 3, model $R^2 = 0.08$-0.15), increased age was again associated with shallowing of LD_{BMO} and LD_{BM} but not with LD_{ASCO} and LD_{Sclera}. Increased BMO area was associated with shallowing of LD_{BM} and LD_{BMO}, and increased ASCO area was associated with shallowing of both LD_{ASCO} and LD_{Sclera}. Increased axial length was again associated with shallowing of LD_{BMO}, LD_{BM}, and LD_{ASCO}. Higher imaging day IOP remained significantly associated with a deeper LD_{Sclera}. LD_{BMO} and LD_{BM} were significantly shallower in female eyes, but LD_{ASCO} and LD_{Sclera} did not demonstrate sex differences. LD_{BM}, LD_{ASCO}, and LD_{Sclera} were each deeper in African descent compared to European and Hispanic descent eyes, which were not different from one another and are considered together in this analysis. LD_{BM} in Asian descent and Native American descent participants (considered together) was also shallower than in African descent eyes. By ANOVA within linear regression models, the
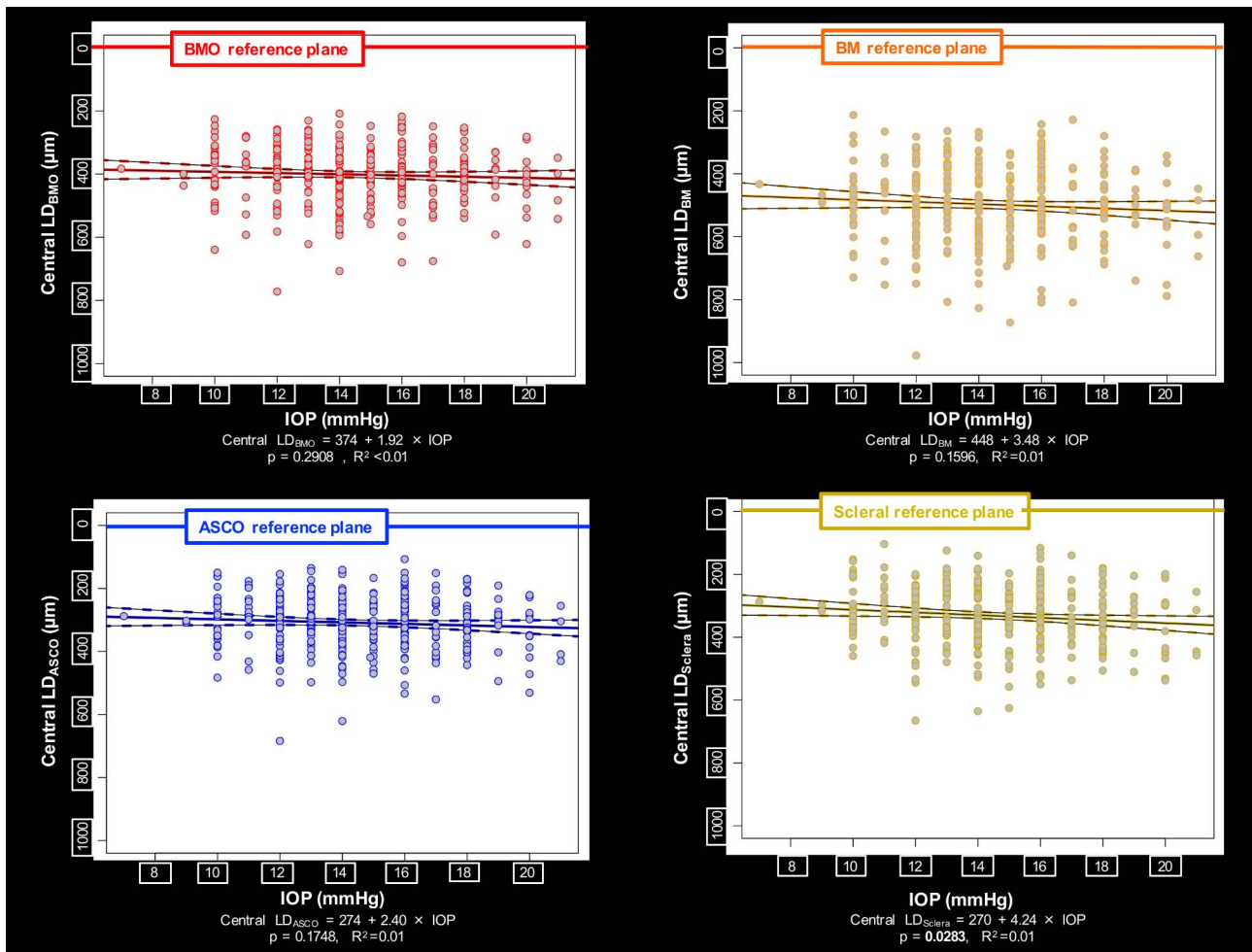
FIGURE 8. Scatter plot and univariate linear regression of laminar depth and IOP. The relationship between laminar depth and IOP is shown, with points *shaded gray* and border line colored according to their reference plane.

proportion of the variance of each laminar depth parameter explained by age, BMO area or ASCO area, axial length, imaging day IOP, sex, and ethnicity, even when significant ($P \leq 0.05$), was small, ranging from 0.2% to 4%.

The population mean values for BMO area and ASCO area, as well as their medians, 95% confidence intervals, and ranges, are reported in Table 2. Within a multivariable regression model (Table 4, model $R^2 = 0.035$–0.039), both BMO area and ASCO area decreased with age, but were not influenced by axial length and were not different by sex. Neither BMO area nor ASCO area was different in African descent compared to European and Hispanic descent eyes. However, the Asian and Native American descent group considered together demonstrated larger BMO area than the African descent group. The population mean values for BMO area and ASCO area are reported by sex in Table 5 and by ethnicity in Table 6. Within a separate multivariable regression model, while European descent versus African descent participants were not significantly different for either BMO or ASCO area, Hispanic descent participants and Asian descent participants each demonstrated larger BMO areas than African descent and European descent participants.

DISCUSSION

The present study characterizes central lamina cribrosa depth in a large healthy population and introduces the use of the

TABLE 5. BMO Area and ASCO Area by Sex

Sex	BMO Area, mm^2, Mean ± SD	ASCO Area, mm^2, Mean ± SD
Female	1.821 ± 0.372	2.253 ± 0.43
Male	1.847 ± 0.398	2.198 ± 0.436

Bolded values indicate statistical significance, $P \leq 0.05$; significantly different from female using a multivariable regression model. SD, standard deviation.

TABLE 6. BMO Area and ASCO Area by Ethnicity

Ethnicity, *n*	BMO Area, mm^2, Mean ± SD	ASCO Area, mm^2, Mean ± SD
European descent, 246	1.784 ± 0.379	2.211 ± 0.438
Hispanic descent, 47	**2.01 ± 0.372**	2.311 ± 0.453
African descent, 47	1.806 ± 0.365	2.205 ± 0.408
Asian descent, 19	**2.093 ± 0.283**	2.358 ± 0.375
Native American, 3	1.744 ± 0.563	1.964 ± 0.266

Bolded values indicate statistical significance, $P \leq 0.05$; significantly different from African descent and European descent, respectively, using a multivariable regression model.

ASCO both as a reference plane for the depth measurement and as the reference perimeter for consistently defining the "central" lamina in all human eyes. In so doing, it reports ocular and demographic effects on three components of ONH phenotype, namely, LD, ASCO area, and BMO area, that will eventually be employed to detect glaucoma and/or its progression in eyes that are at risk for having or developing the disease. Our findings suggest that LD, assessed within the central ASCO, is influenced least by age, axial length, and sex but more by ASCO area when it is measured relative to the ASCO or peripapillary scleral reference planes. However, the magnitude of these effects was similarly small for all reference planes. Laminar depth measurements relative to BMO and BM were deeper in African descent eyes, shallower in females, and shallower as the age and axial length of the eye increased. Laminar depth was also deeper in African descent eyes, and shallower as axial length increased when measured relative to the ASCO but not the sclera. BMO area and ASCO area both decreased with age, and BMO area was greater in Asian descent compared to European descent and African descent participants; however, there were no significant sex- or axial length–related differences in the size of either opening. While the clinical significance of the relatively small effects we describe remain to be determined, our findings provide a foundation for incorporating these anatomic targets into strategies for detecting and staging the optic neuropathy of human glaucoma.

While a plane fit to BMO has become the standard reference for histomorphometric[32,39-41] and OCT-based[32,42] laminar depth measurements, Johnstone et al.[43] were the first to propose that BMO may "migrate" posteriorly (outward) with age, in part due to age-related choroidal thinning. BMO "migration" as a cause of laminar shallowing, in this context, is assumed to be a passive response that is separate from the possibility that the anterior laminar beam insertions "actively" migrate anteriorly as part of age-related laminar remodeling.[44] However, to date, evidence to support the phenomenon of laminar insertion migration is cross-sectional,[1] and longitudinal detection of laminar migration[45] has not been reported."

In our data, older age was significantly associated with a small amount of shallowing in the parameters LD_{BMO} and LD_{BM}, and had smaller effects on LD_{ASCO} and LD_{Sclera} that did not achieve significance. The concept that age-related choroidal thinning contributes to posterior BMO movement is supported by the presence of substantial age-related peripapillary choroidal thinning in these same eyes (Yang H, et al. *IOVS* 2017;58:ARVO E-Abstract 4020) and two recent longitudinal studies.[17,19] Our findings suggest that the effects of peripapillary choroidal thickness on laminar depth are less evident when the ASCO or peripapillary sclera is used as a reference, confirming the original finding of Johnstone et al.[43] for the sclera. Interestingly, our data also suggest that the visibility of the anterior lamina cribrosa increases with age. It is unknown what underlying mechanism causes this result. We speculate that the age-related loss of the prelaminar neural tissues or changes in the material and optical properties associated with age-related laminar stiffening[27,46,47] may contribute to this phenomenon.

Laminar depth was deeper in African descent compared to European and Hispanic descent participants when measured relative to three of four reference planes, which agrees with recent OCT[10] and postmortem[48] studies. Interestingly, African descent participants have substantially thicker peripapillary choroidal thickness in these same eyes (Yang H, et al. *IOVS* 2017;58:ARVO E-Abstract 4020). Rhodes et al.[49] also recently reported that the peripapillary choroid was thicker in African descent participants. Choroidal thickness differences alone might account for this finding for the BMO and BM reference

plane data; however, the fact that laminar depth is deeper in African descent participants when measured relative to the ASCO reference plane strongly suggests that the position of the lamina within the scleral canal is deeper in African descent compared to European and Hispanic descent eyes.

The small age effects on LD that we report are consistent with some OCT studies and disagree with others. Rhodes et al.[10] reported age-related shallowing of mean laminar depth measured relative to BMO in European descent eyes (−2.84 μm/year, $n = 102$, $P < 0.0001$); however, the effect of age was negligible in African descent eyes (−0.08 μm/year, $n = 64$, $P = 0.93$). The findings from the study by Rhodes et al.,[10] which used all segmented anterior laminar surface data points (not just those in the center of BMO), differ modestly in magnitude from the age effects on LD_{BMO} we report here. Similar differences with the results of studies by Seo et al.[18] and Thakku et al.[11] are likely due to the ethnic and methodologic differences between studies. Rhodes et al.[10] also reported a difference between African descent and European descent participants in the direction in which age influences laminar position. This finding is further supported by a separate postmortem study by the same group,[48] but differences in the direction of African descent versus European descent age effects are not present in our data.

The fact that we found no differences in BMO and ASCO area between our European descent and African descent groups disagrees with a series of disc margin–based clinical studies,[50-53] all existing OCT studies of BMO area,[7,54,55] and a recent postmortem 3D reconstruction study,[48] which together suggest that these openings are larger in African descent compared to European descent eyes. The mean values we report for BMO area in European descent eyes are virtually identical to OCT BMO area in 1344 young, predominantly European descent Australian eyes, recently reported by Sanfilippo et al.,[56] the mean BMO area in 116 normal American European descent eyes reported by Rhodes et al.,[7] and the "disc area" using an earlier OCT instrument in 105 normal European descent eyes reported by Girkin et al.[55] However, the mean BMO area for African descent eyes we report is lower than for the African descent eyes of the Rhodes et al.[7] report and two previous OCT reports.[54,55] Possible explanations for this disparity include the small number of African descent participants in our study, and the potential that the racial admixture of the African descent participants in our study (recruited from urban centers) is different from that the Rhodes et al. study, which was performed in retail eye care centers, many of which were centered in rural areas.

The study of Sanfilippo and colleagues[56] found that BMO area was larger in Chinese compared to European descent eyes; and in our study, BMO area was larger in Asian descent compared to European descent eyes by multivariable regression analysis (Table 6). The finding that Asian descent eyes have larger BMO area is further supported by data from a recent study in Japanese subjects with the same instrument[6] (BMO area 2.06 ± 0.45 mm^2 [$n = 258$ subjects]) and a separate study in a Singapore Chinese population with a different instrument, which found the parameter "OCT disc area" to be 1.93 ± 0.37 mm^2 ($n = 466$ subjects).[57] Interestingly, as in our study, OCT BMO area also decreased with age in the Japanese study.[6]

The limitations of this study include the relatively small number of non-European descent participants, which will be addressed by the completion of a 258-participant Japanese normative database,[6] the anticipated completion of the ongoing European and Hispanic subgroup expansions to 250 participants each, and the eventual completion of a planned 250-participant normative database from Mainland China. Our characterization of laminar depth is limited to the central

lamina, however, consistently measuring laminar depth within the central ASCO, rather than taking the mean of all segmented points or using the center of BMO, and is also a strength of this study. Doing so means the laminar sampling area is consistent among all eyes regardless of the degree of BMO/ASCO offset[28] or the variable extent of peripheral laminar segmentation. Variable sampling of the peripheral lamina due to either cause may be most important in the detection of glaucoma, when the lamina is bowed posteriorly and its periphery is anterior to its center. Enhancement of peripheral laminar and anterior scleral surface visualization and its quantification with existing compensation algorithms[58] is planned, and additional studies with swept-source OCT may be indicated. A consistent strategy for laminar visualization and quantification is necessary to evaluate its contribution to the detection of glaucoma and its progression.

Interobserver reproducibility was high for most parameters, however, scleral reference plane nonplanarity reproducibility was only fair. While this finding may follow from the fact that the anterior scleral canal surface reference plane is less planar than the other reference planes (ICC of BMO, BM, ASCO, scleral reference plane nonplanarity were 0.92, 0.99, 0.79, and 0.47, respectively), it is also true that its visualization within OCT B-scans may be less clear for a variety of anatomic reasons including variable size and density of the overlying choroidal septa, the variable size and obliqueness of the penetrating posterior ciliary arteries as they achieve the choroid, and the density or absence of the choroidal scleral interface tissues.[59] However, while the reproducibility of the scleral reference plane was only fair, the reproducibility of LD_{sclera} was good (ICC = 0.98). These data strongly suggest that among the eight reproducibility study eyes, while the distance of the segmented scleral reference plane points above and below the fitted scleral reference plane varied more among the four observers than for the other reference planes, the position of the reference plane in 3D space was not importantly altered by this difference. Thus, while the delineation of the anterior scleral reference plane points may not be as reproducible among observers, our data suggest that the reproducibility of plane positions in 3D space is not importantly altered by this variability. Enhancement of peripheral laminar and anterior scleral surface visualization with existing compensation algorithms[56] is planned, and additional studies with swept-source OCT may be indicated.

Finally, our reproducibility study did not include subjects from every center and therefore does not directly address inter-OCT instrument variability. However, the eight subjects in the reproducibility study did come from three countries (Canada, Germany, and the United States) and represented four of the five ethnicities. To address this concern, we ran a new analysis (general least square regression model in R) to test whether the intra-eye, interobserver variances differed between the three centers that contributed subjects to the reproducibility study (Halifax, Heidelberg, and Baltimore). We performed a regression for each laminar depth parameter on subject ID wherein the variances were allowed to vary between centers (model 1), and then asked whether this analysis fit the data significantly better than a model (model 2) that assumed all centers had the same variance (ANOVA comparisons in R). For all four laminar depth parameters, there were no significant differences between model 1 and model 2, which suggests that the interobserver variances were not different between the three centers.

To provide context for determining the clinical and biomechanical importance of the anatomic targets and reference planes in this study, we propose the following conceptual framework for their interpretation. First, measuring laminar depth relative to BMO or peripapillary BM incorpo-rates choroidal thickness into the measurement, which is both highly variable between subjects and thins over time. Utilizing the ASCO or peripapillary sclera as a reference plane removes this confound, but is dependent upon anatomy that may be more difficult to visualize and reproducibly segment. The clinical implications for the use of each landmark to measure laminar depth in the detection of glaucoma and its progression therefore require further study. Second, segmentation of the ASCO has the potential to incorporate strategies for quantifying ONH tilt and torsion and laminar insertion position within the scleral canal.[3,12,60] Because the lamina primarily inserts into the sclera, and may migrate into the border tissue and pial sheath[44] as part of the optic neuropathy of aging[61,62] and glaucoma,[1,45,60] it is reasonable to propose that measurements of laminar depth, laminar curvature, and laminar insertion position that are intended to inform biomechanical models be based on ASCO rather than BMO. Since IOP-related loading within the peripapillary sclera is delivered to the peripheral lamina via the scleral canal wall,[63] determining the size, shape, and obliqueness of the scleral canal opening (and eventually the canal in its entirety) may provide important insights into the biomechanical components of ONH susceptibility. Finally, the use of the peripapillary scleral surface as a reference plane for the detection of outward or inward ASCO deformation allows detection of outward and inward bowing of the peripapillary sclera in glaucoma[20] and other optic neuropa-thies[64,65] in which IOP and cerebrospinal fluid pressure alterations may be involved.

In summary, in the current study, ocular and demographic effects on central LD were least when it was measured relative to the ASCO and peripapillary sclera, and more common using BMO and peripapillary BM. However, the magnitude of these effects for all four reference planes were small, and their clinical importance in the detection of glaucoma and its progression remains to be determined. While manual segmentation was used in this study, automat-ed segmentation algorithms are in development that will enable the incorporation of central LD and ASCO area into clinical instruments. Characterization of peripapillary cho-roidal thickness (Yang H, et al. *IOVS* 2017;58:ARVO E-Abstract 4020), BMO and ASCO shape, torsion, offset, and tilt, neural canal obliqueness, and peripapillary scleral bowing[1] from the OCT data sets of this study is ongoing and will be the subject of future analyses. Studies to improve glaucoma disease detection, progression detection, and staging by combining LD, BMO area, and ASCO area with existing ONH and RNFL parameters, as well as the emerging targets outlined above, are ongoing.

Acknowledgments

References

1. Yang H, Reynaud J, Lockwood H, et al. The connective tissue phenotype of glaucomatous cupping in the monkey eye - clinical and research implications. *Prog Retin Eye Res*. 2017; 59:1–52.

2. Quigley HA, Green WR. The histology of human glaucoma cupping and optic nerve damage: clinicopathologic correlation in 21 eyes. *Ophthalmology*. 1979;86:1803–1830.

3. Burgoyne C. The morphological difference between glaucoma and other optic neuropathies. *J Neuroophthalmol*. 2015; 35(suppl 1):S8–S21.

4. Armaly MF. Genetic determination of cup/disc ratio of the optic nerve. *Arch Ophthalmol*. 1967;78:35–43.

5. Chauhan BC, Burgoyne CF. From clinical examination of the optic disc to clinical assessment of the optic nerve head: a paradigm change. *Am J Ophthalmol*. 2013;156:218–227, e212.

6. Araie M, Iwase A, Sugiyama K, et al. Determinants and characteristics of Bruch's membrane opening and Bruch's membrane opening-minimum rim width in a normal Japanese population. *Invest Ophthalmol Vis Sci*. 2017;58:4106–4113.

7. Rhodes LA, Huisingh CE, Quinn AE, et al. Comparison of Bruch's membrane opening minimum rim width among those with normal ocular health by race. *Am J Ophthalmol*. 2017; 174:113–118.

8. He L, Ren R, Yang H, et al. Anatomic vs. acquired image frame discordance in spectral domain optical coherence tomography minimum rim measurements. *PLoS One*. 2014;9:e92225.

9. Chauhan BC, Danthurebandara VM, Sharpe GP, et al. Bruch's membrane opening minimum rim width and retinal nerve fiber layer thickness in a normal white population: a multicenter study. *Ophthalmology*. 2015;122:1786–1794.

10. Rhodes LA, Huisingh C, Johnstone J, et al. Variation of laminar depth in normal eyes with age and race. *Invest Ophthalmol Vis Sci*. 2014;55:8123–8133.

11. Thakku SG, Tham YC, Baskaran M, et al. A global shape index to characterize anterior lamina cribrosa morphology and its determinants in healthy Indian eyes. *Invest Ophthalmol Vis Sci*. 2015;56:3604–3614.

12. Lee SH, Kim TW, Lee EJ, et al. Diagnostic power of lamina cribrosa depth and curvature in glaucoma. *Invest Ophthalmol Vis Sci*. 2017;58:755–762.

13. Jung KI, Jung Y, Park KT, et al. Factors affecting plastic lamina cribrosa displacement in glaucoma patients. *Invest Ophthalmol Vis Sci*. 2014;55:7709–7715.

14. Rho CR, Park HY, Lee NY, et al. Clock-hour laminar displacement and age in primary open-angle glaucoma and normal tension glaucoma. *Clin Exp Ophthalmol*. 2012;40: e183–e189.

15. Park SC, Brumm J, Furlanetto RL, et al. Lamina cribrosa depth in different stages of glaucoma. *Invest Ophthalmol Vis Sci*. 2015;56:2059–2064.

16. Furlanetto RL, Park SC, Damle UJ, et al. Posterior displacement of the lamina cribrosa in glaucoma: in vivo interindividual and intereye comparisons. *Invest Ophthalmol Vis Sci*. 2013;54:4836–4842.

17. Vianna JR, Lanoe VR, Quach J, et al. Serial changes in lamina cribrosa depth and neuroretinal parameters in glaucoma: impact of choroidal thickness. *Ophthalmology*. 2017;124: 1392–1402.

18. Seo JH, Kim TW, Weinreb RN. Lamina cribrosa depth in healthy eyes. *Invest Ophthalmol Vis Sci*. 2014;55:1241–1251.

19. Wu Z, Lin C, Crowther M, et al. Impact of rates of change of lamina cribrosa and optic nerve head surface depths on visual field progression in glaucoma. *Invest Ophthalmol Vis Sci*. 2017;58:1825–1833.

20. He L, Yang H, Gardiner SK, et al. Longitudinal detection of optic nerve head changes by spectral domain optical coherence tomography in early experimental glaucoma. *Invest Ophthalmol Vis Sci*. 2014;55:574–586.

21. Ing E, Ivers KM, Yang H, et al. Cupping in the monkey optic nerve transection model consists of prelaminar tissue thinning in the absence of posterior laminar deformation. *Invest Ophthalmol Vis Sci*. 2016;57:2598–2611.

22. Yang D, Fu J, Hou R, et al. Optic neuropathy induced by experimentally reduced cerebrospinal fluid pressure in monkeys. *Invest Ophthalmol Vis Sci*. 2014;55:3067–3073.

23. Burgoyne CF. The non-human primate experimental glaucoma model. *Exp Eye Res*. 2015;141:57–73.

24. Lee KM, Kim TW, Weinreb RN, et al. Anterior lamina cribrosa insertion in primary open-angle glaucoma patients and healthy subjects. *PLoS One*. 2014;9:e114935.

25. Quigley HA, Addicks EM, Green WR, et al. Optic nerve damage in human glaucoma. II. The site of injury and susceptibility to damage. *Arch Ophthalmol*. 1981;99:635–649.

26. Kim YW, Jeoung JW, Kim DW, et al. Clinical assessment of lamina cribrosa curvature in eyes with primary open-angle glaucoma. *PLoS One*. 2016;11:e0150260.

27. Ren R, Yang H, Gardiner SK, et al. Anterior lamina cribrosa surface depth, age, and visual field sensitivity in the Portland Progression Project. *Invest Ophthalmol Vis Sci*. 2014;55: 1531–1539.

28. Downs JC, Yang H, Girkin C, et al. Three-dimensional histomorphometry of the normal and early glaucomatous monkey optic nerve head: neural canal and subarachnoid space architecture. *Invest Ophthalmol Vis Sci*. 2007;48:3195–3208.

29. U.S. Census Bureau. Statistical Abstract of the United States: 2012. Available at: www.census.gov.

30. Spaide RF, Koizumi H, Pozzoni MC. Enhanced depth imaging spectral-domain optical coherence tomography. *Am J Ophthalmol*. 2008;146:496–500.

31. Ivers KM, Yang H, Gardiner SK, et al. In vivo detection of laminar and peripapillary scleral hypercompliance in early monkey experimental glaucoma. *Invest Ophthalmol Vis Sci*. 2016;57:OCT388–OCT403.

32. Strouthidis NG, Grimm J, Williams GA, et al. A comparison of optic nerve head morphology viewed by spectral domain optical coherence tomography and by serial histology. *Invest Ophthalmol Vis Sci*. 2010;51:1464–1474.

33. Yang H, Qi J, Hardin C, et al. Spectral-domain optical coherence tomography enhanced depth imaging of the

normal and glaucomatous nonhuman primate optic nerve head. *Invest Ophthalmol Vis Sci*. 2012;53:394–405.

34. Yang H, He L, Gardiner SK, et al. Age-related differences in longitudinal structural change by spectral-domain optical coherence tomography in early experimental glaucoma. *Invest Ophthalmol Vis Sci*. 2014;55:6409–6420.

35. Fortune B, Reynaud J, Hardin C, et al. Experimental glaucoma causes optic nerve head neural rim tissue compression: a potentially important mechanism of axon injury. *Invest Ophthalmol Vis Sci*. 2016;57:4403–4411.

36. Lockwood H, Reynaud J, Gardiner S, et al. Lamina cribrosa microarchitecture in normal monkey eyes part 1: methods and initial results. *Invest Ophthalmol Vis Sci*. 2015;56:1618–1637.

37. Shrout PE, Fleiss JL. Intraclass correlations: uses in assessing rater reliability. *Psychol Bull*. 1979;86:420–428.

38. McGraw KO, Wong SP. Forming inferences about some intraclass correlation coefficients. *Psychol Methods*. 1996;1:30–46.

39. Yan DB, Coloma FM, Metheetrairut A, et al. Deformation of the lamina cribrosa by elevated intraocular pressure. *Br J Ophthalmol*. 1994;78:643–648.

40. Bellezza AJ, Rintalan CJ, Thompson HW, et al. Deformation of the lamina cribrosa and anterior scleral canal wall in early experimental glaucoma. *Invest Ophthalmol Vis Sci*. 2003;44:623–637.

41. Burgoyne CF, Downs JC, Bellezza AJ, et al. Three-dimensional reconstruction of normal and early glaucoma monkey optic nerve head connective tissues. *Invest Ophthalmol Vis Sci*. 2004;45:4388–4399.

42. Strouthidis NG, Yang H, Fortune B, et al. Detection of optic nerve head neural canal opening within histomorphometric and spectral domain optical coherence tomography data sets. *Invest Ophthalmol Vis Sci*. 2009;50:214–223.

43. Johnstone J, Fazio M, Rojananuangnit K, et al. Variation of the axial location of Bruch's membrane opening with age, choroidal thickness, and race. *Invest Ophthalmol Vis Sci*. 2014;55:2004–2009.

44. Grytz R, Sigal IA, Ruberti JW, et al. Lamina cribrosa thickening in early glaucoma predicted by a microstructure motivated growth and remodeling approach. *Mech Mater*. 2012;44:99–109.

45. Park SC, Kiumehr S, Teng CC, et al. Horizontal central ridge of the lamina cribrosa and regional differences in laminar insertion in healthy subjects. *Invest Ophthalmol Vis Sci*. 2012;53:1610–1616.

46. Albon J, Purslow PP, Karwatowski WS, et al. Age related compliance of the lamina cribrosa in human eyes. *Br J Ophthalmol*. 2000;84:318–323.

47. Albon J, Karwatowski WS, Avery N, et al. Changes in the collagenous matrix of the aging human lamina cribrosa. *Br J Ophthalmol*. 1995;79:368–375.

48. Girkin CA, Fazio MA, Yang H, et al. Variation in the three-dimensional histomorphometry of the normal human optic nerve head with age and race: lamina cribrosa and peripapillary scleral thickness and position. *Invest Ophthalmol Vis Sci*. 2017;58:3759–3769.

49. Rhodes LA, Huisingh C, Johnstone J, et al. Peripapillary choroidal thickness variation with age and race in normal eyes. *Invest Ophthalmol Vis Sci*. 2015;56:1872–1879.

50. Oliveira C, Harizman N, Girkin CA, et al. Axial length and optic disc size in normal eyes. *Br J Ophthalmol*. 2007;91:37–39.

51. Zangwill LM, Weinreb RN, Berry CC, et al. Racial differences in optic disc topography: baseline results from the confocal scanning laser ophthalmoscopy ancillary study to the ocular hypertension treatment study. *Arch Ophthalmol*. 2004;122:22–28.

52. Tsai CS, Zangwill L, Gonzalez C, et al. Ethnic differences in optic nerve head topography. *J Glaucoma*. 1995;4:248–257.

53. Quigley HA, Brown AE, Morrison JD, et al. The size and shape of the optic disc in normal human eyes. *Arch Ophthalmol*. 1990;108:51–57.

54. Knight OJ, Girkin CA, Budenz DL, et al. Effect of race, age, and axial length on optic nerve head parameters and retinal nerve fiber layer thickness measured by Cirrus HD-OCT. *Arch Ophthalmol*. 2012;130:312–318.

55. Girkin CA, Liebmann J, Fingeret M, et al. The effects of race, optic disc area, age, and disease severity on the diagnostic performance of spectral-domain optical coherence tomography. *Invest Ophthalmol Vis Sci*. 2011;52:6148–6153.

56. Sanfilippo PG, Huynh E, Yazar S, et al. Spectral-domain optical coherence tomography-derived characteristics of Bruch membrane opening in a young adult Australian population. *Am J Ophthalmol*. 2016;165:154–163.

57. Tun TA, Sun CH, Baskaran M, et al. Determinants of optical coherence tomography-derived minimum neuroretinal rim width in a normal Chinese population. *Invest Ophthalmol Vis Sci*. 2015;56:3337–3344.

58. Girard MJ, Strouthidis NG, Ethier CR, et al. Shadow removal and contrast enhancement in optical coherence tomography images of the human optic nerve head. *Invest Ophthalmol Vis Sci*. 2011;52:7738–7748.

59. Huynh E, Chandrasekera E, Bukowska D, et al. Past, present, and future concepts of the choroidal scleral interface morphology on optical coherence tomography. *Asia Pac J Ophthalmol (Phila)*. 2017;6:94–103.

60. Yang H, Williams G, Downs JC, et al. Posterior (outward) migration of the lamina cribrosa and early cupping in monkey experimental glaucoma. *Invest Ophthalmol Vis Sci*. 2011;52:7109–7121.

61. Sigal IA, Flanagan JG, Tertinegg I, et al. 3D morphometry of the human optic nerve head. *Exp Eye Res*. 2010;90:70–80.

62. Hogan MJ, Zimmerman LE. The optic nerve. In: MJ, Hogan Zimmerman LE, eds. *Ophthalmic Pathology*. Philadelphia: W.B. Saunders Company; 1969:577–590.

63. Burgoyne CF, Downs JC, Bellezza AJ, et al. The optic nerve head as a biomechanical structure: a new paradigm for understanding the role of IOP-related stress and strain in the pathophysiology of glaucomatous optic nerve head damage. *Prog Retin Eye Res*. 2005;24:39–73.

64. Mader TH, Gibson CR, Pass AF, et al. Optic disc edema, globe flattening, choroidal folds, and hyperopic shifts observed in astronauts after long-duration space flight. *Ophthalmology*. 2011;118:2058–2069.

65. Kupersmith MJ, Sibony P, Mandel G, et al. Optical coherence tomography of the swollen optic nerve head: deformation of the peripapillary retinal pigment epithelium layer in papilledema. *Invest Ophthalmol Vis Sci*. 2011;52:6558–6564.